Investigation into the effect of simulating a 3D cylindrical fluidized bed reactor on a 2D plane

Schalk Cloete, Stein Tore Johansen & Shahriar Amini

1 Abstract

2D planar simulations of 3D cylindrical fluidized bed reactors are routinely carried out in order to reduce computational costs. The error involved in this simplification is largely unknown, however, and this study was therefore conducted to quantify this error over a wide range of reactor operating conditions. 2D and 3D simulations were carried out over a wide range of flow conditions in the bubbling fluidization regime by changing the fluidization velocity, bed mass, reaction temperature and particle size. Detailed comparisons revealed that 2D simulations qualitatively behaved similarly to 3D simulations, but over-predicted reactor performance (measured by the degree of conversion achieved) by about 45% on average. Large systematic variations of this error were also observed with changes in all four independent variables investigated. These large errors were due to two primary factors; incorrect predictions of the gas residence time by misrepresentations of the bed expansion and incorrect predictions of the mass transfer by misrepresentations of bubble formation and the splash zone at the top of the expanded bed. The mass transfer error was found to be most influential and was also confirmed as the most important factor to be correctly predicted by CFD simulations. 3D predictions of the mass transfer resistance were further analysed to identify the particle size as a very influential variable through which the mass transfer characteristics in fluidized bed reactors can be influenced.

2 Introduction

Fluidized bed reactors find application in a wide range of process industries dealing with gas-solid or solid catalysed reactions. The fluid-like behaviour of these reactors results in excellent heat and mass transfer performance which is highly favourable for any reactor process. Fluidized bed reactors can be very challenging to design and scale up, however, and commercialisation of processes utilising such reactors therefore typically consists of a large number of incremental scale-up and demonstration steps. For this reason, there is a great need for modelling tools that can be used to reduce the risk of taking larger scale-up steps.

The fundamental flow modelling framework of computational fluid dynamics (CFD) is considered in this work to be a viable methodology for achieving this purpose. CFD inherently accounts for the complex and tightly interconnected non-linear interactions between reactor hydrodynamics, heat transfer, species transfer and reaction kinetics. Because of this fundamental basis, it is reasoned that CFD can provide the generality demanded of a modelling tool used for fluidized bed reactor design, optimization and scale-up.

CFD simulations face their own challenges, however. The primary challenge is presented by the mesoscale structure formation characteristic of any fluidized bed reactor process. Small clusters of particles are formed within these beds due to the non-linear drag interaction between the gas and solids and have a very large influence on all physics occurring within the reactor. Due to the small time and

length scales at which these structures occur, computational grid and time step requirements impose very stringent limitations on the size of reactor that can be realistically simulated with today's computational resources. If grid sizes are made too large to resolve the structures, the reactor physics is not resolved and predictions can become grossly inaccurate [1].

Work is underway to develop filtered closure laws which can model the effects of these mesoscale structures and thereby allow grid sizes larger than the structures themselves (e.g. [2]). Such approaches can facilitate a simulation speed up to several orders of magnitude. Accurate modelling of the mesoscale structures is highly complex, however, and will require thorough validation before it can be safely used. Currently, closure laws are available for hydrodynamics only and at least a similar closure law for reaction kinetics will be required before this approach can be used for complete reactor simulations.

In the absence of such filtered approaches, a popular methodology for simulating fluidized bed reactors has been to carry out the simulations in 2D instead of 3D. Axissymmetric 2D simulations are not a viable option because cylindrical coordinates cannot accurately capture the mesoscale structures. The resolution of the structures demands that the grid size is constant throughout the entire bed. Therefore, planar 2D simulations are the only viable option.

Depending on the flow problem being simulated, this planar 2D approximation can result in computational cost savings around two orders of magnitude. By making this assumption, however, this simulated geometry is made substantially different from the real cylindrical 3-D geometry in two primary ways. Firstly, the mesoscale structures are now 2D in nature and are expected to have a different influence on the flow than they would have in 3D. Secondly, the spanwise direction in 2D differs substantially from the axial direction in 3D.

Despite the substantial geometrical differences, favourable comparisons to 3D cylindrical experimental results using 2D planar simulations have been achieved for riser flows by scaling for the flux and superficial velocity passing through the riser [3]. For reactive flows, however, such an approach would not be viable because it alters the ratio of gaseous and solid reactants being fed to the reactor. Therefore, no such scaling is possible in reactive simulations.

This study was therefore completed in order to quantify the error that would result from simulating a reactive 3D fluidized bed on a 2D plane. Simulations were carried out both in 2D and 3D over a wide range of flow variables including gas flow rate, bed height, reaction temperature and particle size. Such a holistic comparison should give a clear indication of the degree to which the 2D assumption jeopardises the generality of the model.

3 Nomenclature

Main Symbol definitions:

α	Volume fraction
ϕ	Kinetic energy transfer rate (kg/m.s^3)
γ	Dissipation rate (kg/m.s^3)
Θ_s	Granular temperature (m^2/s^2)
ρ	Density (kg/m^2)
ς	Specularity coefficient

$\bar{\bar{\tau}}$	Stress tensor (kg/m.s^2)
$\vec{\tau}_s$	Particle shear force at the wall (N)
$\vec{\upsilon}$	Velocity vector (m/s)
Ω	Resistance (s)
∇	Del operator / Gradient (1/m)
C	Molar concentration (mol/m^3)
d	Diameter (m)
$\vec{g}$	Gravity vector (m/s^2)
$g_{0,ss}$	Radial distribution function
$\bar{\bar{I}}$	Identity tensor
$\vec{J}$	Diffusive flux (kg/(m^2.s))
K	Momentum exchange coefficient (kg/(m^3.s)
k	Diffusion coefficient (kg/m.s)
k	Reaction rate constant (m/s)
M	Molar mass (kg/mol)
N	Moles (mol)
p	Pressure (Pa)
R	Gas constant (8.314 J/K.mol)
R^H	Heterogeneous reaction rate (mol/m^{3}s)
S	Source term (kg/m^{3}s)
T	Temperature (K)
t	Time (s)
$\vec{U}_{s,\|\|}$	Particle velocity parallel to wall (m/s)
V	Volume (m^3)
x	Mass fraction

Sub- and superscript definitions:

0	Inlet or initial
Θ_s	Granular temperature
ave	Average
A	Species A
c	Unreacted core
$\exp$	Expanded
g	Gas or grain
gs	Inter-phase
i	Species index
$\max$	Maximum packing
n	Reaction order
R	Reaction rate
MT	Mass transfer
res	Residence
s	Solids

Abbreviations:

by	Interaction
d	Particle diameter (µm)
H	Initial static bed height (m)
KTGF	Kinetic Theory of Granular Flows
L	Linear effect
Q	Quadratic effect
SS	Sum of squares
T	Temperature (°C)
TFM	Two Fluid Model
U	Fluidization velocity (m/s)

4 Simulations

The simulations in this study were carried out according to the well documented Eulerian-Eulerian Two Fluid Model (TFM) closed by the Kinetic Theory of Granular Flows (KTGF).

4.1 Model equations

An abbreviated version of the governing equations will be given below. The full equation set is presented elsewhere [1].

4.1.1 Conservation equations

The continuity and momentum equations for the gas phase are solved as follows:

$$\frac{\partial}{\partial t}\left(\alpha_g \rho_g\right)+\nabla\cdot\left(\alpha_g \rho_g \vec{\upsilon}_g\right)=0 \qquad \text{Equation 1}$$

$$\frac{\partial}{\partial t}\left(\alpha_g \rho_g \vec{\upsilon}_g\right)+\nabla\cdot\left(\alpha_g \rho_g \vec{\upsilon}_g \vec{\upsilon}_g\right)=-\alpha_g \nabla p+\nabla\cdot\bar{\bar{\tau}}_g+\alpha_g \rho_g \vec{g}+K_{sg}\left(\vec{\upsilon}_s-\vec{\upsilon}_g\right) \qquad \text{Equation 2}$$

The TFM assumes the solids to also be a continuum and solves similar equations for this phase:

$$\frac{\partial}{\partial t}\left(\alpha_s \rho_s\right)+\nabla\cdot\left(\alpha_s \rho_s \vec{\upsilon}_s\right)=0 \qquad \text{Equation 3}$$

$$\frac{\partial}{\partial t}\left(\alpha_s \rho_s \vec{\upsilon}_s\right)+\nabla\cdot\left(\alpha_s \rho_s \vec{\upsilon}_s \vec{\upsilon}_s\right)=-\alpha_s \nabla p-\nabla p_s+\nabla\cdot\bar{\bar{\tau}}_s+\alpha_s \rho_s \vec{g}+K_{gs}\left(\vec{\upsilon}_g-\vec{\upsilon}_s\right) \qquad \text{Equation 4}$$

The solids stresses $\left(p_s \text{ and } \bar{\bar{\tau}}_s\right)$ are modelled according to the KTGF which will be briefly discussed in the next section. Inter-phase momentum exchange $\left(K_{gs}=K_{sg}\right)$ was modelled according to the formulation of Syamlal and O'Brian [4].

Species are conserved only for the gas phase.

$$\frac{\partial}{\partial t}\left(\alpha_g \rho_g x_{gi}\right)+\nabla\cdot\left(\alpha_g \rho_g \vec{\upsilon}_g x_{gi}\right)=\nabla\cdot\alpha_g \vec{J}_{gi}+\alpha_g S_{gi} \qquad \text{Equation 5}$$

No energy conservation was included under the assumption of isothermal flow. This is usually a good assumption due to the excellent mixing achieved in fluidized bed reactors.

4.1.2 The kinetic theory of granular flows

The KTGF [4-6] was implemented to model solids stresses resulting from particle collisions and subscale particle motions. Kinetic energy contained in the random particle motions is quantified in terms of granular temperature and can be written in conservation form as follows:

$$\frac{3}{2}\left[\frac{\partial}{\partial t}\left(\alpha_s\rho_s\Theta_s\right)+\nabla\cdot\left(\alpha_s\rho_s\vec{\upsilon}_s\Theta_s\right)\right]=\left(-p_s\bar{\bar{I}}+\bar{\bar{\tau}}_s\right):\nabla\vec{\upsilon}_s+\nabla\cdot\left(k_{\Theta_s}\nabla\Theta_s\right)-\gamma_{\Theta_s}+\phi_{gs} \qquad \text{Equation 6}$$

In the present study, this equation was solved in its algebraic form by neglecting the contributions of convection (second term on the left) and diffusion (second term on the right). This is a good assumption in dense and slow moving bubbling beds [7] since the local generation (first term on the right), dissipation due to inelastic collisions (third term on the right) [5] and damping by the primary phase (final term) [6] strongly outweigh contributions from convective and diffusive fluxes.

The granular temperature is subsequently used to calculate values of the solids viscosity which are used in the solids stress tensor. Bulk viscosity [5] and the three components of shear viscosity, collisional [4, 6], kinetic [6] and frictional [8], were considered in the calculations.

Normal stresses modelled according to the solids pressure used in Equation 4 as well as in Equation 6 is calculated according to Lun *et al.* [5]. The radial distribution function which is a measure of the average distance between particles is a central concept in the KTGF and is calculated according to Ogawa and Oshima [9].

4.1.3 Reaction kinetics

Reaction kinetics were implemented using the shrinking core model [10] with chemical kinetics as the rate limiting step. A simple, catalytic conversion of gas species A to gas species B was simulated to occur on the surface of microscopic solid grains (*S*) within the particles used in the fluidized bed:

$$A+S\rightarrow B+S$$

The physical and chemical properties of species A and B were specified to be identical (that of air) so that the reaction would not influence the hydrodynamics resulting in a non-linear interaction. This will significantly simplify the interpretation of results, enabling clear conclusions regarding hydrodynamic and reaction kinetic behavior to be drawn from each simulation.

When reaction rate control is assumed with the shrinking core model, the rate of consumption of species A on the surface of the unreacted core can be expressed as follows:

$$-\frac{dN_A}{dt}=\pi d_c^2 k C_A^n \qquad \text{Equation 7}$$

This relation can be rewritten in terms of a volumetric heterogeneous reaction rate that can be implemented into the CFD code:

$$R^H=-\frac{1}{V}\frac{dN_A}{dt}=\frac{6}{d_g}\alpha_s k C_A=\frac{6}{d_g}\alpha_s k\left(\frac{x_A\rho_g}{M_A}\right) \qquad \text{Equation 8}$$

Equation 8 is formulated on the assumption that the reaction takes place at an equal rate on all the grains inside the particle. The catalytic reaction simulated also implied no shrinkage of the unreacted core. A first order reaction was simulated.

The hypothetical reaction rate constant in Equation 9 was implemented. Both the pre-exponential factor and the activation energy are representative of real materials used in reacting fluidized bed systems such as Chemical Looping Combustion.

$$k = 0.1e^{(-100000/RT)} \qquad \text{Equation 9}$$

The reaction rate in each cell (molar rate of change from species A to species B per unit volume) was then implemented as a source term into Equation 5. Since the species had identical properties and the reaction occurred in a 1:1 stoichiometric ratio, no mass or momentum source terms were required. The source term in Equation 5 was taken as $S_{gi} = R^H M_i$ for the product species (B) and $S_{gi} = -R^H M_i$ for the reactant species (A).

4.1.4 Boundary Conditions

A simple no-slip wall boundary condition was set for the gas phase. The Johnson and Jackson [11] boundary condition was used for the granular phase with a specularity coefficient of 0.5.

$$\vec{\tau}_s = -\frac{\pi}{6}\sqrt{3}\varsigma\frac{\alpha_s}{\alpha_{s,\max}}\rho_s g_{0,ss}\sqrt{\Theta_s}\vec{U}_{s,\|} \qquad \text{Equation 10}$$

A velocity inlet condition was specified according the specific simulation run in question. The incoming gas consisted of pure reactant (species A). The outlet was specified as a pressure outlet at atmospheric pressure.

4.1.5 Flow solver and solver settings

The commercial software package, FLUENT 13.0 was used as the solver. The phase coupled SIMPLE scheme [12] was used for pressure-velocity coupling and the higher order QUICK scheme [13] for the spatial discretization of all remaining equations. First order implicit temporal discretization was used. It has been shown that 2nd order time discretization is necessary for accurate solution of fast-moving riser flows with the TFM [1], but this is not the case for dense bubbling beds where the vast majority of the bed moves relatively slowly.

4.1.6 Geometry and meshing

A 2D planar geometry, 0.28 m in width and 2 m in height, was used to simulate the fluidized bed. The bed dimensions and flow conditions were based on a hydrodynamically validated simulation [14] in order to increase confidence in model results. The geometry was divided into two zones: the bed zone with a height of 1.8 m and a porous zone for the remaining 0.2 m. The porous zone was specified in the top region in order to achieve a plug flow and prevent any backflow occurring at the outlet.

The domain was meshed with structured, 5 mm cells as was used in the aforementioned validation study [14]. As shown in Figure 1, this grid size achieved satisfactory, albeit not perfect, grid independence for the simulation run at the centre of the central composite design completed in this study (see section 5 for more information). It would be desired to use a finer grid, but 5 mm was the minimum size that could realistically be afforded to carry out the full 3D simulations conducted in this study.

The 3D simulations were completed on a cylindrical geometry, 0.28 m in diameter and 2 m in height so as to allow for a direct comparison with the 2D planar simulations. The geometry was originally meshed with perfectly cubical 2 cm cells using the cut-cell method and subsequently refined twice to 5 mm in the lower region where the bed resides in order to minimize the number of cells.

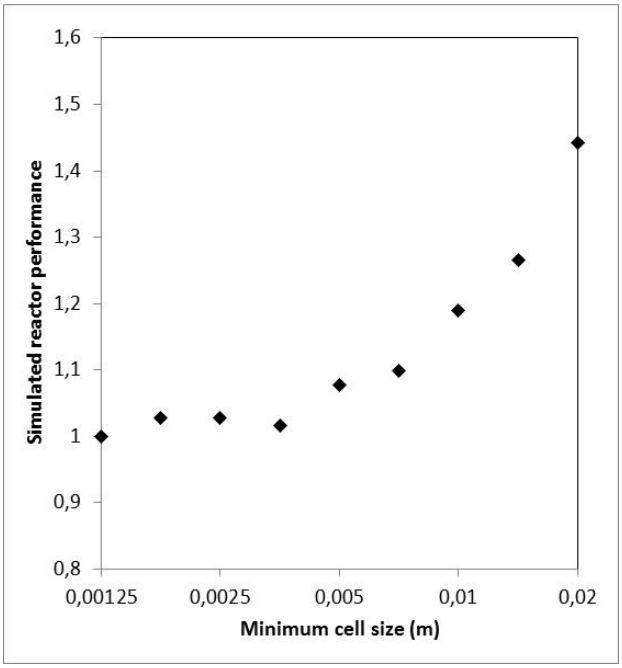

Figure 1: The sensitivity of the overall reactor performance (-log(x_A) at the outlet) to changes in the mesh size.

4.1.7 Simulation summary

A summary of the physical properties and simulation parameters are given in Table 1.

Table 1: Physical properties and simulation parameters

Gas density (A and B)	0.3 kg/m^3
Gas viscosity (A and B)	3x10^{-5} kg/m·s
Particle density	2500 kg/m^3
Grain diameter	1 µm
Bed width/diameter	0.28 m
Bed height	2 m
Particle-particle restitution	0.9
Specularity coefficient	0.5
Initial solids packing	0.60
Maximum packaging limit	0.63
Mesh size	5 mm

5 Methods

The results and subsequent analysis was based on a four factor central composite design [15]. This is a form of experimental design (also applicable to simulation experiments) where the response of specific dependent variables to changes in various independent variables can be easily assessed, accurately quantified and visualized. The four independent variables, henceforth called factors, considered in the design were specified over five levels as follows:

- Gas flow rate (U). This factor was varied between 0.2 m/s and 1 m/s in 0.2 m/s intervals. These velocities produced fluidization falling in the lower to central regions of the bubbling fluidization regime. Lower fluidization velocities are expected to increase reactor performance (defined as a degree of gas conversion achieved) due to an increase in the gas residence time.
- Static bed height (H). The initial height of the bed was also varied between 0.2 and 1 m in 0.2 m intervals. This range was chosen to facilitate direct comparison to the effect of gas flow rate. Similarly to the gas flow rate, an increase in the static bed height is expected to increase reactor performance by increasing the gas residence time.
- Reactor temperature (T). This factor was varied between 700 and 900°C in 50°C intervals. When implemented into Equation 9, this 200°C increase resulted in a factor 8.2 increase in the reaction rate constant which will improve reactor performance.
- Particle diameter (d). This factor was varied between 200 and 600 µm in 100 µm intervals and therefore represents typical Geldart B powder which is usually used in bubbling fluidized beds. The size of the particles used in fluidization has a large impact on the hydrodynamics, but also the reaction kinetics. Larger particle sizes are expected to decrease the expanded bed height, but also increase the rate of mass transfer from the bubble to the emulsion phase.

The effects of changes in these factors on reactor performance were evaluated in terms of three dependent variables:

- Reactor performance expressed as $-\log\left(x_A\right)$ where x_A is the fraction of species A (reactant) exiting the reactor unreacted. This result can be interpreted as a measure of the residence time required to convert the reactant to a certain degree when all other factors influencing reaction rate are kept constant. In this case, for a first order reaction, the rate of change of the reacting species mass fraction would be expressed as follows: $dx/dt = -Cx$ which can be integrated to from $x = 1$ at $t = 0$ to find the time at a certain final conversion as $t = -C^{-1}\ln\left(x\right)$. In this case it was assumed that $C^{-1} = \log\left(e\right)$ in order to express the reactor performance as $-\log\left(x\right)$. The base 10 logarithm was chosen simply to make the results easier to interpret. For instance, 0% conversion would return a reactor performance of $-\log\left(1\right) = 0$, 90% conversion would return a reactor performance of $-\log\left(0.1\right) = 1$, 99% conversion a reactor performance of $-\log\left(0.01\right) = 2$ etc. In practice, this measure linearizes reactor performance and makes it possible to distinguish between cases which achieve high conversions.
- Bed expansion ratio calculated as the expanded bed height divided by the initial static bed height. The expanded bed height was derived from time averaged data collected in the CFD model and was assumed to be located at a time-averaged solids volume fraction of 0.05.
- Normalized total pressure drop over the bed which is quantified as the ratio of the total pressure drop to the pressure required to counter the total weight of the particles. Since the reactor outlet pressure was set to zero, the total pressure drop was calculated as the area-weighted average pressure over the reactor inlet. This pressure was then divided by the pressure needed to support the weight of the solids in the bed.

The central composite design was run for the 2D and the 3D geometry. Each completion of the central composite design required 26 simulation experiments, filling the four dimensional parameter space with

the reactor performance as predicted by the particular geometry simulated. This facilitated a direct and easily quantifiable comparison between the results attained with the 2D and the 3D geometry. Results presented and discussed below will mostly focus on quantifying the differences between these two geometries.

Results will primarily be displayed in two ways: an analysis of variance (ANOVA) and response surfaces of dependent variables to changes in various factors. The ANOVA will be used to identify the most significant factors in the design (i.e. the factors where the different modelling methodologies give significantly different predictions).

The significance of factors will be defined by the p-value which is an indication of the probability of the observed effect to result purely by random chance. If this value becomes small $\left(p < 0.05\right)$, the effect is said to be significant because the probability of it arising from pure chance is fairly small. A value of $p < 0.01$ is generally regarded as highly significant. The p-value is calculated from the F-test which weighs the amount of explained variance in the design against the amount of unexplained variance (experimental error, rounding error, averaging error, data not fitting the second order model etc.). This ratio can then be evaluated as a p-value to decide whether the variance is caused by a significant effect or is simply random.

The relative variance explained by each factor will also be given as the percentage of the total sum of squares (SS). The total sum of squares is the sum of all the squared distances between the various data points and the mean. A larger total sum of squares implies that the data are scattered wide around the mean and there is a lot of variance in the design. This measure will give an indication of the importance of significant effects relative to each other.

Once the significant effects are identified in this way, the difference between 2D and 3D simulation predictions will be plotted on a response surface as a function of these highly significant factors in order to gain an understanding of the nature of various differences between the 2D and 3D simulations.

6 Results and discussion

Results will be presented in four sections. Firstly, the results from the 2D and 3D simulations will be presented and briefly analysed. Then the differences between these results will be quantified and analysed. Subsequently, deeper investigations into the reactor performance will be conducted in a more detailed analysis. And finally, some more detailed investigations on the mass transfer resistance will be presented. The data collected from the simulations on which this discussion will be based is given in Table 2.

Table 2: Simulation results from the two central composite designs.

Case	Fluidization velocity (m/s)	Static bed height (m)	Reactor temperature (°C)	Particle size (µm)	2D simulations			3D simulations		
					Reactor performance	Bed expansion ratio	Normalized pressure drop	Reactor performance	Bed expansion ratio	Normalized pressure drop
1	0.4	0.4	750	300	0.573	1.548	0,962	0.442	1.450	0,978
2	0.4	0.4	750	500	0.983	1.223	0,980	0.830	1.253	0,999
3	0.4	0.4	850	300	1.097	1.555	0,960	0.796	1.453	0,979
4	0.4	0.4	850	500	2.206	1.223	0,988	1.559	1.255	0,992
5	0.4	0.8	750	300	0.917	1.419	0,960	0.642	1.343	0,972
6	0.4	0.8	750	500	1.893	1.164	0,980	1.373	1.204	0,995
7	0.4	0.8	850	300	1.703	1.410	0,961	1.072	1.356	0,970
8	0.4	0.8	850	500	4.088	1.176	0,980	2.427	1.195	0,995
9	0.8	0.4	750	300	0.305	2.158	0,948	0.246	1.795	0,970
10	0.8	0.4	750	500	0.445	1.740	0,963	0.365	1.563	1,007
11	0.8	0.4	850	300	0.551	2.163	0,946	0.441	1.828	0,969
12	0.8	0.4	850	500	0.900	1.705	0,952	0.676	1.588	1,007
13	0.8	0.8	750	300	0.509	1.891	0,949	0.366	1.639	0,973
14	0.8	0.8	750	500	0.793	1.595	0,957	0.654	1.474	1,014
15	0.8	0.8	850	300	0.893	1.879	0,945	0.627	1.654	0,965
16	0.8	0.8	850	500	1.593	1.574	0,968	1.077	1.459	1,002
17	0.2	0.6	800	400	4.356	1.042	0,997	2.489	1.102	0,999
18	1.0	0.6	800	400	0.585	2.022	0,946	0.440	1.700	0,998
19	0.6	0.2	800	400	0.456	1.760	0,961	0.361	1.600	0,984
20	0.6	1.0	800	400	1.483	1.466	0,960	1.016	1.400	0,992
21	0.6	0.6	700	400	0.472	1.575	0,956	0.365	1.467	0,986
22	0.6	0.6	900	400	1.759	1.558	0,936	1.180	1.473	0,989
23	0.6	0.6	800	200	0.548	2.047	0,957	0.533	1.680	0,973
24	0.6	0.6	800	600	1.572	1.310	0,973	1.224	1.288	1,008
25 (C)	0.6	0.6	800	400	0.987	1.570	0,961	0.733	1.483	0,994
26 (C)	0.6	0.6	800	400	1.007	1.553	0,959	0.719	1.477	0,993

6.1 2D and 3D results

Firstly, the results from the 2D and 3D simulations will be analysed. The ANOVA for the CFD predictions of reactor performance $\left(-\log\left(x_A\right)\right)$ and bed expansion ratio are given in Table 3. Linear, Quadratic and interaction effects are reported. A significant linear effect implies that reactor performance increases or decreases linearly with changes in the specific factor. If a significant quadratic effect is present, this implies that the response is curved (not simply a straight line). A significant interaction effect occurs when the reactor performance changes significantly when two factors are changed simultaneously.

Table 3: ANOVA table summarizing the response of 2D and 3D simulation results to changes in the four factors investigated. Significant factors are shown in bold, while highly significant factors are shown in bold italics. The factors are denoted by U (fluidization velocity), H (static bed height), T (reactor temperature) and d (particle diameter). Different effects are indicated by L (linear), Q (quadratic) and by (interaction).

Effect	2D performance		3D performance		2D bed expansion ratio		3D bed expansion ratio		2D normalized pressure drop		3D normalized pressure drop	
	SS (%)	p-value	SS (%)	p-value	SS (%)	p-value	SS (%)	p-value	SS (%)	p-value	SS (%)	p-value
U(L)	***38.22***	***0.0000***	***39.49***	***0.0000***	***65.02***	***0.0000***	***62.45***	***0.0000***	***52.45***	***0.0000***	0.51	0.4613
U(Q)	**8.06**	**0.0064**	***6.03***	***0.0046***	***0.72***	***0.0000***	0.06	0.0760	3.56	0.0807	0.09	0.7594
H(L)	***9.24***	***0.0042***	***8.99***	***0.0012***	***7.60***	***0.0000***	***5.68***	***0.0000***	0.00	0.9902	0.00	0.9537
H(Q)	0.10	0.7094	0.15	0.5904	**0.07**	**0.0187**	**0.10**	**0.0298**	0.08	0.7809	1.86	0.1733
T(L)	***14.31***	***0.0009***	***14.85***	***0.0002***	0.03	0.0914	0.01	0.3781	1.39	0.2555	0.42	0.5047
T(Q)	0.00	0.9865	0.01	0.9122	0.01	0.4655	0.00	0.9668	3.92	0.0687	1.81	0.1783
d(L)	***11.96***	***0.0018***	***16.66***	***0.0001***	***25.55***	***0.0000***	***29.62***	***0.0000***	***24.47***	***0.0004***	***77.21***	***0.0000***
d(Q)	0.02	0.8785	0.10	0.6626	0.01	0.3862	***0.57***	***0.0001***	0.78	0.3885	0.94	0.3236
U(L) by H(L)	1.18	0.2252	0.61	0.2850	***0.40***	***0.0000***	***0.53***	***0.0001***	0.50	0.4882	0.35	0.5383
U(L) by T(L)	2.05	0.1181	1.45	0.1105	0.02	0.2101	0.01	0.3468	0.22	0.6414	0.23	0.6196
U(L) by d(L)	2.95	0.0671	**3.53**	**0.0204**	***0.14***	***0.0027***	**0.29**	**0.0012**	1.29	0.2726	**6.30**	**0.0214**
H(L) by T(L)	0.75	0.3276	0.26	0.4793	0.02	0.1354	0.00	0.9235	0.35	0.5615	0.29	0.5780
H(L) by d(L)	1.39	0.1907	1.34	0.1238	***0.31***	***0.0001***	***0.52***	***0.0001***	0.01	0.9330	0.26	0.5997
T(L) by d(L)	1.90	0.1313	1.25	0.1350	0.03	0.1208	0.00	0.6554	0.39	0.5354	0.10	0.7477
Error	7.86		5.29		0.10		0.17		10.60		9.64	0.0000
Total	100.0		100.0		100.0		100.0		100.0		100.0	

When looking at Table 3, the immediate reaction is that, with the possible exception of the normalized pressure drop, the two geometrical representations produce very similar responses to changes in the four factors investigated, suggesting that the 2D approximation is reasonable.

The comparisons between the 2D and the 3D geometry become less favourable, however, when one considers the mean and the standard deviation of the four sets of data in Table 2:

- 2D reactor performance: 1.26±1.00
- 2D bed expansion ratio: 1.59±0.30
- 2D normalized pressure drop: 0.96±0.014
- 3D reactor performance: 0.87±0.57
- 3D bed expansion ratio: 1.47±0.18
- 3D normalized pressure drop: 0.99±0.014

It is clear that, relative to the 3D case, the reactor performance is significantly over-predicted on the 2D geometry (by 44.3%) and the data is scattered much wider around the mean (74.9% wider). For the bed expansion ratio, the 2D simulations predict the bed to be 8.3% higher on average and the data is scattered 64.5% wider around the mean. These are some highly significant differences and will be analysed in greater detail in the subsequent sections.

The normalized pressure drop, on the other hand, shows very little difference between the 2D and 3D cases. The 2D mean is only 3.1% lower than the 3D mean and the standard deviation is identical. This similarity is to be expected since the scope for great variation in the normalized pressure drop is very limited. The only factor capable of influencing the normalized pressure drop is the friction at the walls and this force is expected to be small relative to the weight of the solids. However, even though the degree of variation in the data is small, Table 3 clearly shows some highly significant effects of the fluidization velocity and the particle size on the normalized pressure drop. These effects also merit further investigation.

Firstly, however, the response of the reactor to changes in the four factors investigated will be analysed in order to better understand the behaviour of the reactor. This will be done via the response surfaces for the 3D results shown in Figure 2 and Figure 3.

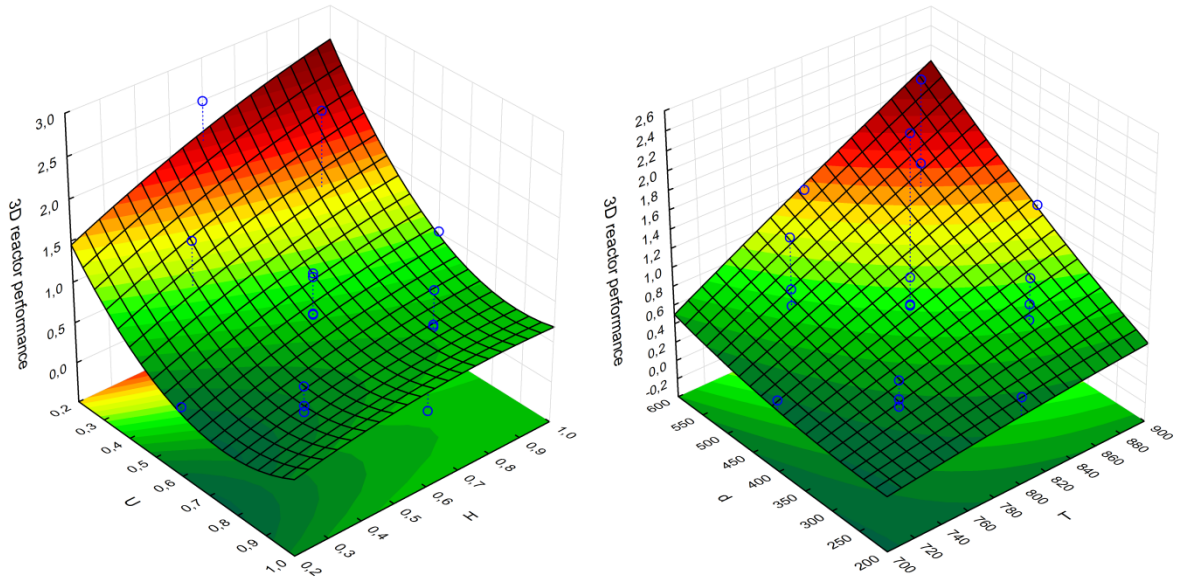

Figure 2: Response of reactor performance (-log(x_a)) to changes in the four factors investigated.

The simulation results are much the same as those reported by [16], but a summary will be given here. Figure 2 visualizes the observation from Table 3 that the fluidization velocity is the most influential factor on reactor performance and also the only factor with a significant quadratic effect. Reactor performance increases at an ever increasing rate as the fluidization velocity is reduced. This is due to the gas residence time being inversely proportional to the fluidization velocity.

Despite being varied over the same range as the fluidization velocity, the static bed height had a much smaller influence on results, primarily because the mass transfer resistance from bubble growth in fluidized bed reactors reduces the performance gains that can be made by using taller beds. For lower fluidization velocities, on the other hand, the gains in gas residence time are enhanced by the formation of smaller bubbles.

Reactor performance increased linearly with temperature despite the reaction rate increasing exponentially with an increase in temperature. This implies that the bubble-to-emulsion mass transfer limitation becomes increasingly significant as the temperature is increased and serves to nullify the exponential increase in reaction rate.

The reactor performance also showed a linear increase with an increase in particle size. Note that the reaction rate was not a function of particle size, but of a constant grain size in all particles. This increase is a result of improved bubble-to-emulsion mass transfer at larger particle sizes since larger slip velocities can be attained. Gaseous reactant from the bubbles can therefore penetrate the emulsion more effectively when larger particle sizes are used.

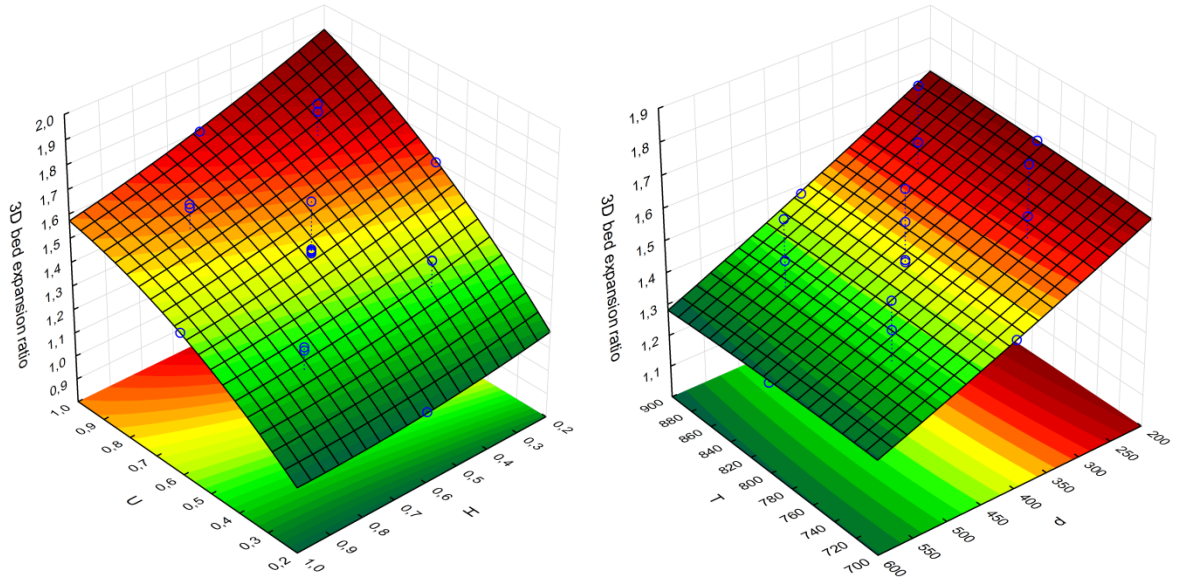

Figure 3: Response of the bed expansion ratio to changes in the four factors investigated.

For the bed expansion ratio, Figure 3 confirms that fluidization velocity and particle diameter are the most influential factors. Responses are in the expected directions. A minor increase in bed expansion ratio is also observed with a decrease in static bed height. This can be understood by acknowledging that smaller bubbles form close to the distributor and grow as they rise along the bed. As the bubbles grow, the bubble velocity increases and the gas residence time decreases. Hence, a shorter bed will have a smaller mean bubble size, leading to slower bubble rise velocities and a more expanded bed.

When looking at the normalized pressure drop, Table 3 indicates that only the linear effect of particle size and the interaction effect between fluidization velocity and particle size is significant. The influence of these two factors is displayed in Figure 4 where it is clear that the pressure drop over the bed is very similar to the pressure needed to counter the weight of the particles at low fluidization velocities, but a linear trend of greater pressure drop for larger particles becomes increasingly clear as the fluidization velocity is increased. At low fluidization velocities, motion in the bed is relatively gentle and friction at the walls does not play a major part, but more vigorous fluidization creates more motion in the bed and therefore the potential for a greater contribution of wall friction to the overall pressure drop. From the data, it appears that the motion at the wall is primarily downwards for smaller particle sizes (leading to a lower pressure drop) and primarily upwards for larger particle sizes (leading to a larger pressure drop).

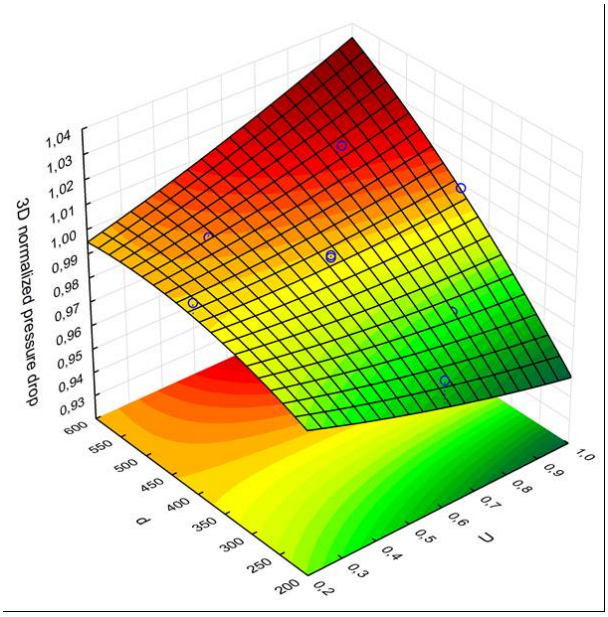

Figure 4: Response of the normalized pressure drop to changes in fluidization velocity (U) and particle diameter (d).

6.2 Differences between 2D and 3D

The differences between the 2D and 3D simulations were calculated as the percentage by which any specific variable (χ) calculated in the 2D simulation is larger than in 3D. More explicitly:

$$diff = \left(\frac{\chi_{2D}}{\chi_{3D}} - 1 \right) \times 100\% \qquad \text{Equation 11}$$

This ratio was calculated for each of the 26 pairs of cases considered in the two central composite designs and subsequently used in a new central composite design to show how this ratio varies with changes in the four factors investigated. This transformation will clearly indicate any systematic inconsistencies between 2D and 3D simulations.

Three new central composite designs were composed from Equation 11 where χ was taken first as the reactor performance, then as the expanded bed expansion ratio and finally as the normalized pressure drop. ANOVA results for these two central composite designs are displayed below.

Table 4: ANOVA table summarizing differences between 2D and 3D model responses to changes in the four factors investigated. Significant factors are shown in bold, while highly significant factors are shown in bold italics. The factors are denoted by U (fluidization velocity), H (static bed height), T (reactor temperature) and d (particle diameter). Different effects are indicated by L (linear), Q (quadratic) and by (interaction).

Effect	Reactor performance		Bed expansion ratio		Normalized pressure drop	
	SS (%)	p-value	SS (%)	p-value	SS (%)	p-value
U(L)	***21,32***	***0,0008***	***57,79***	***0,0000***	***51,75***	***0,0001***
U(Q)	**5,91**	**0,0358**	0,03	0,5905	2,14	0,2579
H(L)	***21,73***	***0,0008***	***2,19***	***0,0009***	0,00	0,9678
H(Q)	0,01	0,9096	0,13	0,3013	2,23	0,2490
T(L)	***19,82***	***0,0011***	0,37	0,0922	0,25	0,6913
T(Q)	0,11	0,7458	0,02	0,6844	0,35	0,6407
d(L)	1,41	0,2676	***34,46***	***0,0000***	**11,58**	**0,0181**
d(Q)	***9,41***	***0,0117***	***2,56***	***0,0005***	2,90	0,1922
U(L) by H(L)	1,36	0,2760	0,30	0,1245	0,01	0,9394
U(L) by T(L)	1,53	0,2498	0,30	0,1234	0,00	0,9940
U(L) by d(L)	0,01	0,9184	0,00	0,8991	**10,38**	**0,0235**
H(L) by T(L)	1,29	0,2884	0,06	0,4792	1,00	0,4321
H(L) by d(L)	0,05	0,8299	**0,56**	**0,0441**	0,15	0,7553
T(L) by d(L)	4,65	0,0575	0,02	0,6456	0,70	0,5100
Error	11,38		1,20		16,55	
Total	***21,32***		***57,79***		100,00	

Table 4 shows a large number of significant systematic differences in reactor predictions by the 2D and 3D modelling approaches. Further insight can be gained from response surfaces displayed in Figure 5.

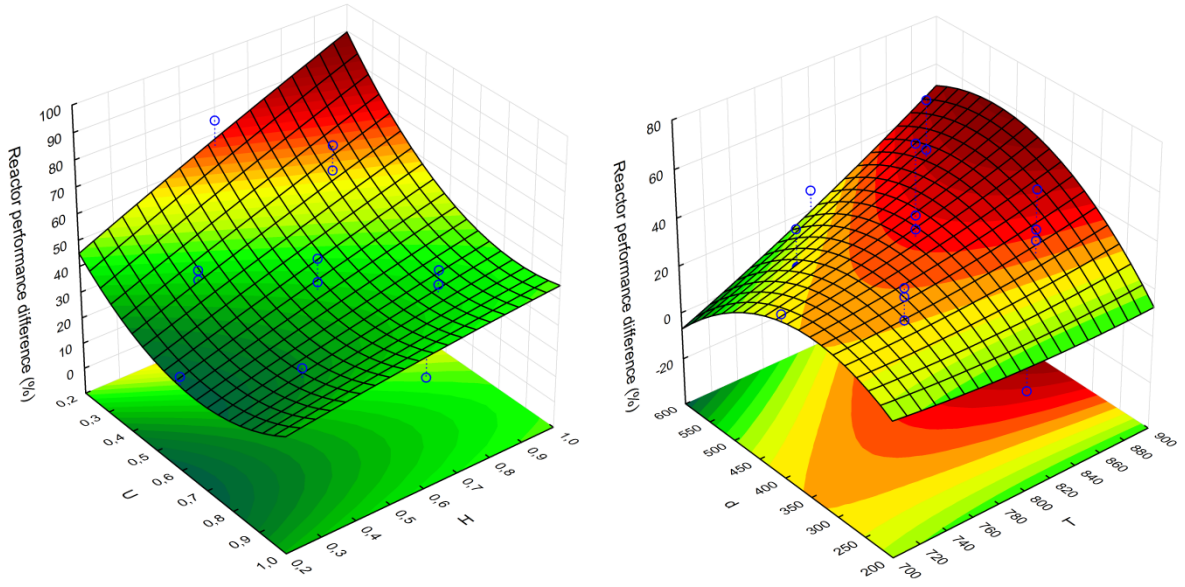

Figure 5: Response of the difference between 2D and 3D reactor performance to changes in the four factors investigated. Differences should be interpreted as the percentage by which the 2D reactor performance is greater than the 3D reactor performance.

Aside from confirmation that the 2D model predicted substantially better reactor performance than the 3D model and that the difference between predictions by the 2D and 3D approaches are strongly dependent on all flow variables, Figure 5 is quite hard to interpret. The parabolic response of reactor performance difference to changes in the particle size is especially interesting. Further discussion on these responses is postponed to the following section.

It is clear, however, that the differences between 2D and 3D model predictions are large and vary significantly with changes in all factors. This can be part of the reason why a recent 2D validation study [17] against experimental data collected from a 3D pilot scale reactor [18] could not achieve a satisfactory match over a range of different fluidization velocities. In that study, it was found that the model gave good predictions of reactor performance at higher fluidization velocities, but over-predicted reactor performance at lower velocities. Figure 5 clearly shows that the 2D simulation increasingly over-predicts reactor performance relative to the 3D simulations as the fluidization velocity is decreased.

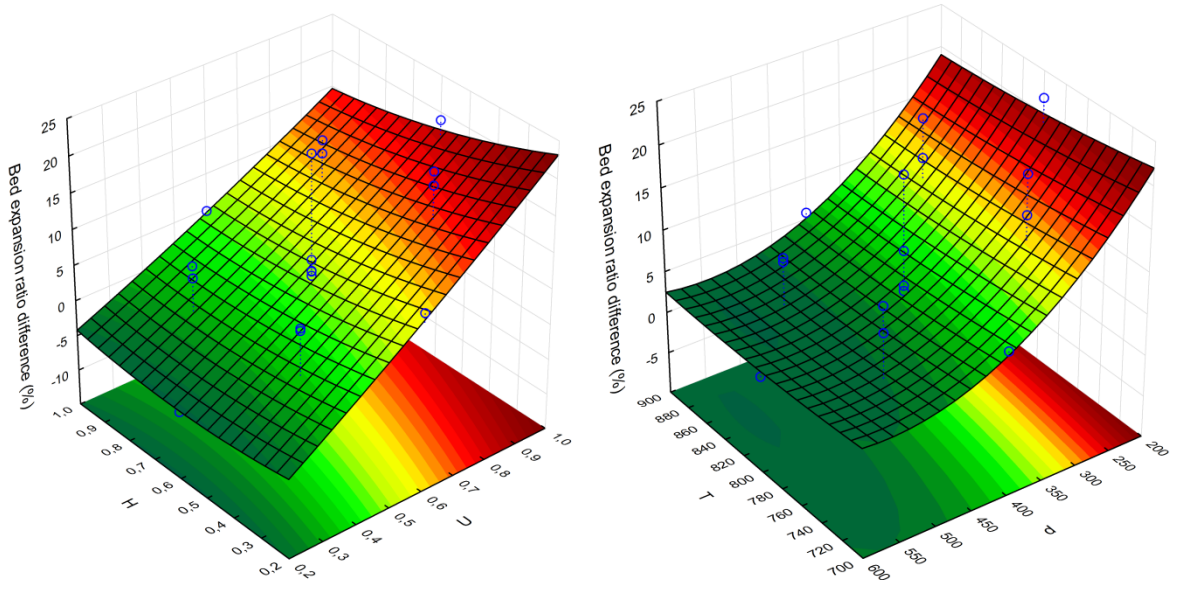

Figure 6: Response of the difference between 2D and 3D bed expansion ratio to changes in the four factors investigated. Differences should be interpreted as the percentage by which the 2D bed expansion ratio is greater than the 3D bed expansion ratio.

The differences in predictions of static bed height are displayed in Figure 6 where the nature of the effects of the two most significant factors in Table 4, the fluidization velocity and the particle size, can clearly be seen. It is shown that, as the fluidization velocity is increased, the 2D approximation increasingly over-predicts the bed height relative to the 3D simulations. A similar effect is seen for reductions in the particle size.

This is a direct result of the geometrical differences between the 2D and 3D domains. As the bubbling becomes more vigorous, the mean flow structure increasingly assumes a core-annulus structure as can be seen in Figure 7. A core-annulus flow structure forces more particles towards the wall regions of the reactor which represent a much larger percentage of the reactor volume in 3D than in 2D. Thus, for the same mass of solids, a core annular flow structure in 3D will cause less bed expansion than a similar flow structure in 2D as can be seen from Figure 6.

The response to changes in fluidization velocity is linear, implying that the degree of core-annular flow increases linearly with gas flow rate. A quadratic response is observed for the particle size, however. This is due to the distinct difference in the manner in which the flow field is resolved between 2D and 3D as will be discussed in the analysis of the difference in normalized pressure drop discussed below.

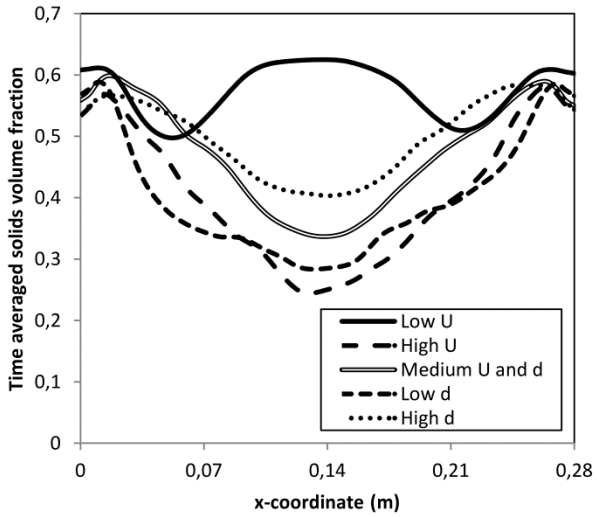

Figure 7: Cross-stream solids volume fraction profiles at a height of 0.5 m for cases 17 (low U), 18 (high U), 23 (low d), 24 (high d) and 25 (medium U and d) in Table 2.

The difference in the response of the normalized pressure drop in the 2D and 3D simulations is displayed in Figure 8 where it is clear that simulations with low fluidization velocities and small particle sizes behave very similarly. Simultaneous increases in fluidization velocity and particle size, however, cause the 2D pressure drop to become progressively smaller relative to the 3D pressure drop. This implies that, under these circumstances, the 2D simulations display substantial downflows at the walls (thereby creating an upwards frictional force supporting some of the weight of the particles) while Figure 4 showed that the 3D simulations tend to show upflow at the walls under these circumstances.

For further illustration, the time averaged velocity and solids volume fraction profiles of two cases; case 5 (small U and d) and case 14 (large U and d) in Table 2, are displayed in Figure 9 and Figure 10. It is clear that, in both cases, the 2D simulations show a much stronger recirculatory flow pattern then the 3D simulations although this difference is more pronounced in case 14. Figure 10 also confirms that radial solids volume fraction segregation (the driving force behind the solids recirculation) is much more pronounced in 2D than in 3D. The choice of geometry therefore has a very large influence on the hydrodynamics in the bed.

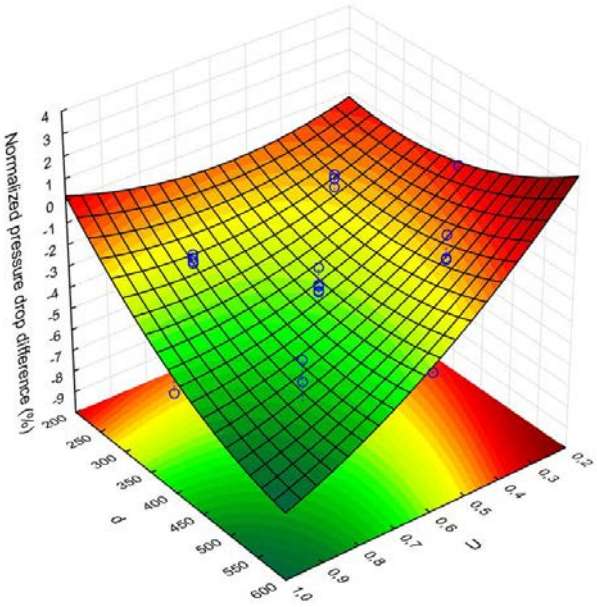

Figure 8: Response of the difference between the 2D and 3D normalized pressure drop to changes in fluidization velocity (U) and particle size (d). Differences should be interpreted as the percentage by which the 2D normalized pressure drop is greater than the 3D normalized pressure drop.

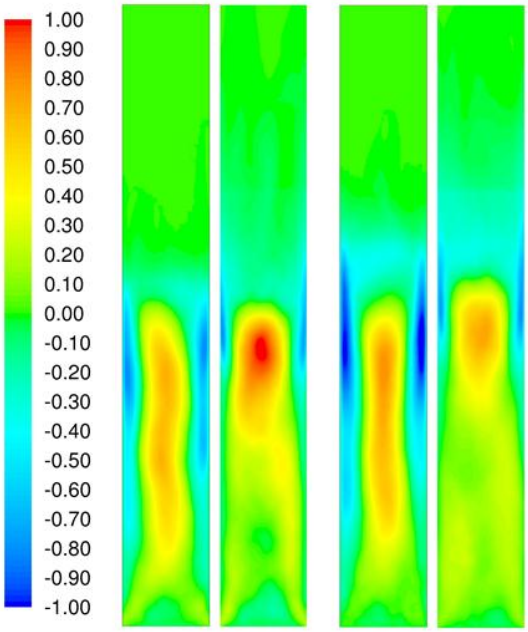

Figure 9: Time averaged vertical solids velocity contours for case 5 (two images on the left) and case 14 (two images on the right). I each pair of images, the image on the left is the 2D simulation and the one on the right is the 3D simulation.

If the recirculatory flow pattern was resolved similarly in the 2D and 3D cases, it would be expected that the pressure drop in the 3D case would be smaller than in the 2D case since the ratio between the wall area and the reactor volume is larger, thereby allowing for more wall friction. This is the reason why the normalized pressure drops returned by 2D and 3D in case 5 are quite similar even though the recirculatory flow pattern is significantly stronger in 2D than in 3D.

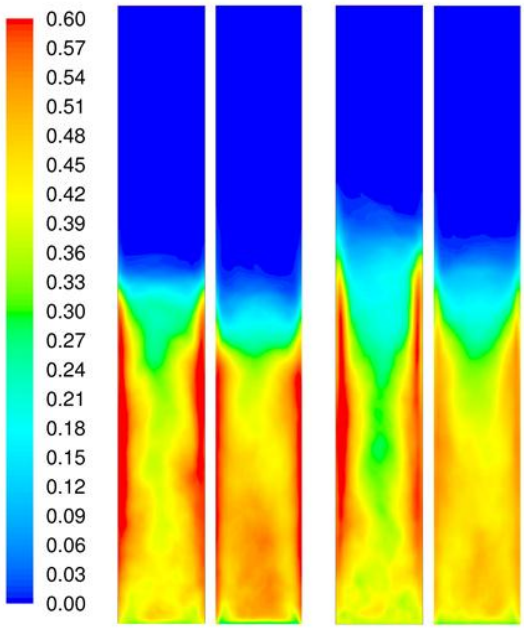

Figure 10: Time averaged solids volume fraction contours for case 5 (two images on the left) and case 14 (two images on the right). I each pair of images, the image on the left is the 2D simulation and the one on the right is the 3D simulation.

Finally, it is clear that the very limited radial segregation occurs in the 3D case especially for larger particle sizes. This is the reason for the similar bed expansion ratios returned by the 2D and 3D simulations when larger particle sizes are used (Figure 6)

6.3 Decomposition of reactor performance

The trends shown in Figure 5 require further in-depth analysis in order to form an adequate understanding of geometry-related differences in reactor performance. A much clearer picture can be gained by breaking reactor performance down into more fundamental constituents. For a bubbling fluidized bed reactor, performance is influenced by three factors: the gas residence time, the reaction rate on the particle level and the quality of the mass transfer of reactant gas to the particles. Gas residence time is influenced by the height of the bed and the fluidization velocity, particle reaction rate is influenced by the reaction temperature, and the rate of mass transfer is influenced by the bubble characteristics (primarily influenced by gas velocity and particle size) and the permeability of the emulsion phase (primarily influenced by particle size).

The CFD model predicts the gas residence time (by means of the bed expansion) as well as the mass transfer (by resolving the bubbles and directly transporting gaseous reactants into the emulsion phase). The reaction rate on the particle, however, is fed into the model as a closure law and needs to be determined by external experiments (mostly TGA studies) or molecular modelling. 2D and 3D results will therefore differ in their predictions of gas residence time and mass transfer, but will be identical in their predictions of particle reaction rate since the same closure law is implemented in both sets of simulations.

It will therefore be a worthwhile exercise to compare simulation performance with regards to the predicted gas residence time and the predicted mass transfer. The gas residence time will be calculated as a function of the expanded bed height. The height of the expanded bed influences the gas residence time in two ways: by changing the distance that the gas has to travel and by changing the velocity with

which the gas travels. A more compact bed will give the gas a shorter distance over which to react and also increase the gas velocity by presenting a smaller void fraction through which the gas must travel. Thus, the gas residence time is calculated as follows:

$$t_{res} = \frac{H_{\exp}}{U_0 / \alpha_{g,ave}} = \frac{H_{\exp}}{U_0 / \left(1 - 0.6\, H_0 / H_{\exp}\right)} \qquad \text{Equation 12}$$

Equation 12 finds the gas residence time by dividing the distance that the gas has to travel with the average velocity by which this distance is travelled. The value 0.6 signifies the initial solids volume fraction of the initial static bed.

The mass transfer resistance predicted by the CFD models was calculated by comparing the simulated reactor performance to the reactor performance that would occur if there was no phase segregation (i.e. uniform volume fraction and therefore no bubble-to-emulsion mass transfer resistance). Reactor performance under perfect mixing was calculated as follows with the volume fractions taken as constant averages within the expanded bed:

$$\left(-\ln\left(x_A\right)\right)_{perfect} = \frac{t_{res}}{\alpha_{g,ave}} \frac{6}{d_g} \alpha_{s,ave} k \qquad \text{Equation 13}$$

Here, the natural logarithm was used instead of the base 10 logarithm simply as a matter of algebraic convenience. The relation in Equation 13 was attained by integrating the transient evolution of the mass fraction (Equation 14) over the time $\left(t_{res}\right)$ needed to traverse the height of a uniformly packed, perfectly mixed reactor:

$$\alpha_{g,ave} \frac{dx_A}{dt} = \frac{6}{d_g} \alpha_{s,ave} k x_A \qquad \text{Equation 14}$$

In Equation 13, only the reaction rate on the grain surface area is limiting the rate of conversion. This reaction rate resistance can be seen as the inverse of the expanded reaction rate constant which now includes the constant solids volume fraction and grain diameter: $\Omega_R = d_g / 6\alpha_{s,ave} k$. Thus, Equation 13 can be rewritten as:

$$\left(-\ln\left(x_A\right)\right)_{perfect} = \frac{t_{res} / \alpha_{g,ave}}{\Omega_R} \qquad \text{Equation 15}$$

In reality, however, another resistance in the form of the mass transfer resistance $\left(\Omega_{MT}\right)$ is added in series to the reaction rate resistance. Thus:

$$\left(-\ln\left(x_A\right)\right)_{real} = \frac{t_{res} / \alpha_{g,ave}}{\Omega_R + \Omega_{MT}} \qquad \text{Equation 16}$$

Since the gas residence time based on the superficial velocity $\left(t_{res} / \alpha_g\right)$ is constant between the perfect and real cases, the known values of the reactor performance from both sets of simulations can be used to calculate the mass transfer resistance:

$$\Omega_{MT} = \left(\frac{\left(-\ln\left(x_A\right)\right)_{perfect}}{\left(-\ln\left(x_A\right)\right)_{real}} - 1 \right) \Omega_R = \left(\frac{\left(-\ln\left(x_A\right)\right)_{perfect}}{\left(-\ln\left(x_A\right)\right)_{real}} - 1 \right) \frac{d_g}{6\alpha_{s,ave} k} \qquad \text{Equation 17}$$

Using Equation 12 and Equation 17, the gas residence times and mass transfer resistances for each of the 2D and 3D runs were calculated and then compared according to Equation 11. These results were then analysed in two central composite designs yielding the ANOVA results reported in Table 5.

Table 5: ANOVA table summarizing the response of differences between 2D and 3D representations of the gas residence time and the mass transfer resistance to changes in the four factors under investigation. Significant factors are shown in bold, while highly significant factors are shown in bold italics. The factors are denoted by U (fluidization velocity), H (static bed height), T (reactor temperature) and d (particle diameter). Different effects are indicated by L (linear), Q (quadratic) and by (interaction).

Effect	Residence time		Mass transfer	
	SS (%)	p-value	SS (%)	p-value
U(L)	***59.08***	***0.0000***	***29.27***	***0.0001***
U(Q)	0.07	0.4831	2.14	0.1280
H(L)	***1.63***	***0.0040***	3.37	0.0631
H(Q)	0.13	0.3257	0.06	0.7877
T(L)	0.39	0.1031	0.04	0.8256
T(Q)	0.03	0.6128	0.41	0.4840
d(L)	***33.70***	***0.0000***	***48.08***	***0.0000***
d(Q)	***2.25***	***0.0013***	**6.27**	**0.0167**
U(L) by H(L)	0.14	0.3166	0.13	0.6979
U(L) by T(L)	0.33	0.1312	0.06	0.7860
U(L) by d(L)	0.38	0.1077	0.77	0.3441
H(L) by T(L)	0.07	0.4657	0.16	0.6635
H(L) by d(L)	0.39	0.1021	0.33	0.5293
T(L) by d(L)	0.04	0.5832	0.25	0.5877
Error	1.36		8.67	
Total	100.00		100.00	

The results in Table 5 indicate a complete dominance by the factors of fluidization velocity and particle size. The ANOVA results for the difference in predictions of gas residence time are very similar to that of the bed height in Table 4. This is understandable since the differences in the gas residence time predictions of 2D and 3D simulations are influenced only by the differences in bed height predictions according to Equation 12. When comparing Figure 6 and Figure 11, it can be seen that these responses are almost identical, except for the fact that the response of gas residence time is steeper because of the added effect of increasing gas velocities in more compact beds.

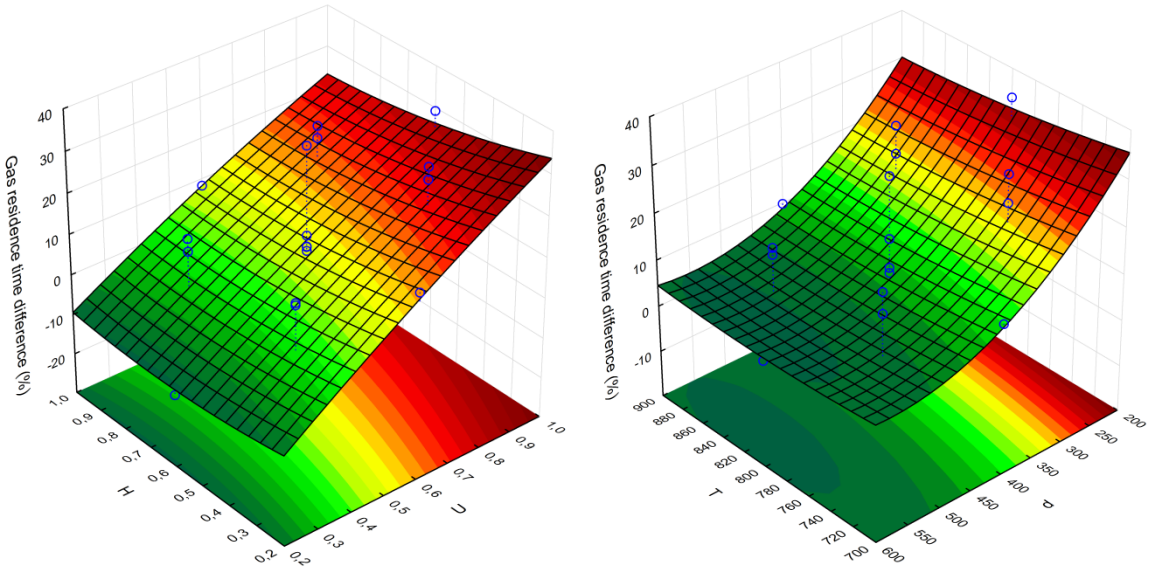

Figure 11: Response of the difference between 2D and 3D gas residence times to changes in the four factors investigated. Differences should be interpreted as the percentage by which the 2D gas residence time is greater than the 3D gas residence time.

When analyzing the differences in mass transfer resistance predictions by 2D and 3D models, Table 5 indicates that the effect of temperature is totally absent and the effect of bed height is also insignificant. This is understandable since the reactor temperature has no direct influence on the mass transfer resistance. The bed height might possibly have a small effect on mass transfer by influencing bubble growth, but Table 5 indicates that this small effect is predicted similarly by the 2D and 3D models. Significant differences are observed in response to changes in the fluidization velocity and the particle size as illustrated in Figure 12.

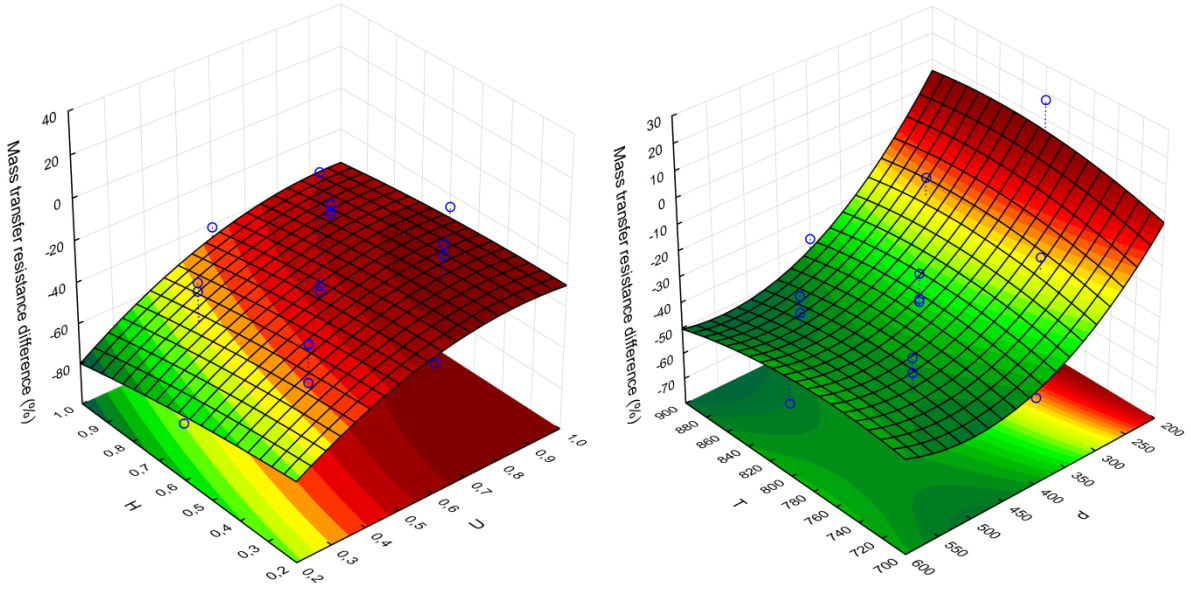

Figure 12: Response of the difference between 2D and 3D mass transfer resistances to changes in the four factors investigated. Differences should be interpreted as the percentage by which the 2D mass transfer resistance is greater than the 3D mass transfer resistance.

Figure 12 indicates that the mass transfer resistance predicted by the 2D model becomes progressively smaller in relation to the 3D predictions as the fluidization velocity is deceased. This effect is really large at low flowrates with the 2D mass transfer resistance being as much as 80% (5 times) smaller than the 3D mass transfer resistance. As Figure 13 indicates, the geometrical constraints cause the 2D simulations to be unable to resolve the small bubbles close to the inlet, thereby greatly enhancing the mass transfer in this region.

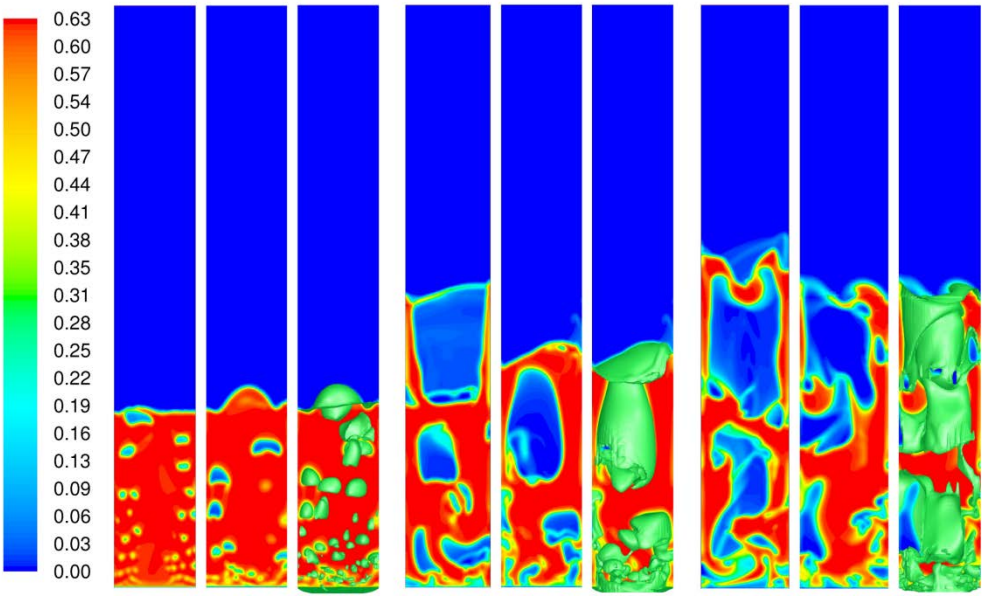

Figure 13: Particle volume fraction contours for a low (left), medium (centre) and high (right) fluidization velocity. For each case, the picture on the left shows the 2D simulation, while the two remaining pictures show the 3D simulation with and without visualized bubbles.

Figure 13 does not provide sufficient insight into the reasons why the 2D mass transfer resistance is still 40% smaller than the 3D mass transfer resistance at higher flowrates though. It appears as if the bubble sizes in the 2D and 3D cases are comparable at higher fluidization velocities. If anything, the 3D mass transfer should be greater for equally sized bubbles because the third dimension grants additional surface area to a 3D bubble through which mass transfer can occur.

Further insight into this question can be attained from analyzing the evolution of the reactor performance through the length of the reactor. The data was assembled from time averaged reactant (species A) mass fractions through the bed calculating a time averaged reactor performance $\left(-\log\left(x_A\right)\right)$ in every cell. In addition, this value was weighed with the local time averaged void fraction in order for reactor performance values in the core region of the reactor where a lot of gas rises to have a larger weight. The reactor performance indicator was therefore calculated as $-\log\left(x_A\right)\alpha_{g,ave}$ in every cell and averaged in spanwise space (a horizontal line in 2D and a horizontal disk in 3D) at several heights within the 2D and 3D reactors for case 25 in Table 2. The resulting plot is shown in Figure 14.

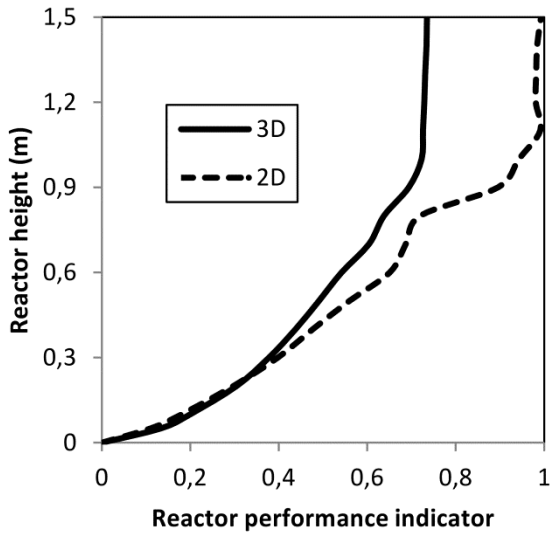

Figure 14: Evolution of the reactor performance along the height of the reactor for case 25 solved both in 2D and 3D.

Interestingly, it is observed that the reactor performance predictions in the lower reactor regions are very similar in 2D and 3D despite the clear differences in the macroscopic flow patterns observed in Figure 9. In the upper reactor regions, however, the trends start diverging before splitting sharply in the splash region at the top of the expanded bed (the expanded bed height was 0.94 m in 2D and 0.89 m in 3D). It appears as if the splash region has a much greater effect on the 2D simulations than on the 3D simulations. The reason for this is that the gas can exit the bed much more cleanly in 3D, but appears to get trapped to some degree in 2D due to the missing degree of freedom. A barrier of solids is often formed in front of an exiting bubble such as that shown for the 2D case at the medium fluidization velocity in Figure 13. It appears as if this exit effect is primarily responsible for the persistent 40% reduction in overall mass transfer resistance in the 2D case.

The response to the changes in particle size is related to the bubble shape and size resolved in 2D and 3D simulations. Figure 15 indicates that 3D simulations with the small particle size created substantially smaller bubbles than 2D simulations. This allowed the 3D simulations to decrease in mass transfer resistance and even display a lower mass transfer resistance than the 2D simulations for the case with the finest particles (Figure 12). When the particle size is increased, however, the bubble behavior becomes similar again and the 2D mass transfer resistance returns to more than 40% that of the 3D mass transfer resistance.

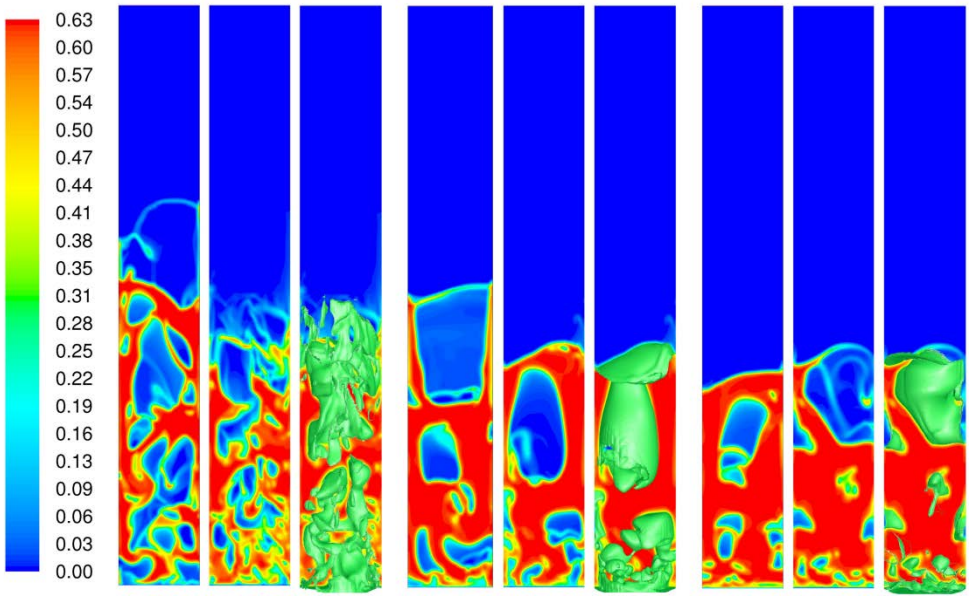

Figure 15: Particle volume fraction contours for a small (left), medium (centre) and large (right) particle size. For each case, the picture on the left shows the 2D simulation, while the two remaining pictures show the 3D simulation with and without visualized bubbles.

When considering Figure 11 and Figure 12 in combination, the interesting quadratic response of the difference in reactor performance predicted by the 2D and 3D approaches in Figure 5 can be explained. Figure 11 indicates that the gas residence time predicted by the 2D model increases faster with decreases in the particle size than that predicted by the 3D model, implying that the 2D model will increasingly over-predict the reactor performance in relation to the 3D case with decreases in the particle size. Figure 12, on the other hand, shows that the 2D under-prediction of the mass transfer resistance rapidly decreases with decreases in particle size, implying that the 2D model will increasingly over-predict the reactor performance with increases in the particle size. These two discrepancies will therefore strive to cancel each other out, resulting in the response observed in Figure 5.

A similar effect can be observed for the fluidization velocity. In relation to the 3D cases, the 2D simulations tend to increasingly over-predict reactor performance with increases in fluidization velocity caused by increases in the gas residence time, but simultaneously increasingly over-predict reactor performance with decreases in fluidization velocity due to under-predictions of the mass transfer resistance. Figure 5 indicates that the mass transfer resistance is the stronger of these factors because the overall difference in predictions of reactor performance shows that the 2D model increasingly over-predicts reactor performance with decreases in fluidization velocity.

This trend was also aided by the mechanism that is responsible for the factors of bed height and temperature to show highly significant effects on the difference between 2D and 3D predictions of reactor performance (Table 4). These effects are surprising because no direct errors in the 2D predictions of gas residence time and mass transfer resistance to changes in these two factors could be identified in Table 5. It can be reasoned, however, that these effects are caused simply because Figure 12 indicates that 2D predictions of the mass transfer resistance are generally significantly smaller than 3D predictions. Factors that influence the gas residence time and particle reaction rate (i.e. fluidization velocity, bed height and temperature) will therefore be more efficient in 2D simulations where the mass transfer resistance plays less of a role and thereby cause sharper responses to changes in these factors.

This postulate can be confirmed in Figure 5 where it is shown that 2D over-predictions of reactor performance increase with increases in gas residence time (decreases in fluidization velocity and increases in static bed height) as well as with increases in particle reaction rate (increases in temperature).

Due to this indirect effect, the under-predictions of the mass transfer resistance are identified as the primary shortcoming of 2D-planar simulations. This misrepresentation of the mass transfer rate not only has a direct influence on model responses to factors influencing the bubble size and shape (e.g. fluidization velocity and particle size), but also an indirect influence on factors affecting gas residence time and particle reaction rate (e.g. fluidization velocity, static bed height and temperature).

6.4 Further investigations into the mass transfer resistance

In acknowledgment of the importance of the mass transfer in fluidized bed reactors, some further discussion on this topic will now be presented. It is of great industrial interest to ensure that the mass transfer resistance in fluidized bed reactors is as low as possible and it will therefore be interesting to investigate the effect of the four factors on the ratio between the mass transfer and reaction rate resistances as defined in Equation 17. Thus, this ratio $\left(R_{MT}/R_R\right)$ was defined as the dependent variable and the central composite design for the 3D runs was repeated to yield the ANOVA results in Table 6.

Table 6: ANOVA table summarizing the response of the ratio of mass transfer to reaction rate resistance to changes in the four factors under investigation. Significant factors are shown in bold, while highly significant factors are shown in bold italics. The factors are denoted by U (fluidization velocity), H (static bed height), T (reactor temperature) and d (particle diameter). Different effects are indicated by L (linear), Q (quadratic) and by (interaction).

Effect	SS (%)	p-value
U(L)	0,02	0,8133
U(Q)	0,00	0,9699
H(L)	***11,87***	***0,0001***
H(Q)	0,00	0,9607
T(L)	***34,16***	***0,0000***
T(Q)	0,76	0,1762
d(L)	***41,51***	***0,0000***
d(Q)	0,04	0,7486
U(L) by H(L)	0,10	0,6045
U(L) by T(L)	0,01	0,8851
U(L) by d(L)	1,58	0,0616
H(L) by T(L)	1,12	0,1077
H(L) by d(L)	**2,40**	**0,0262**
T(L) by d(L)	**2,42**	**0,0256**
Error	4,01	
Total	100.00	

Table 6 shows that all factors apart from the fluidization velocity has an influence on the ratio of mass transfer to reaction rate resistance. This is somewhat counter-intuitive since one would reason that mass transfer characteristics should change significantly as changes in the fluidization velocity affect the bubble behavior. In this case, however, it would seem that these factors cancel each other out perfectly over the range of data investigated. The two primary cancelling effects in this case are the reduction of

bubble size with reductions in fluidization velocity and the increased agitation and mixing in the bed caused by increases in fluidization velocity.

Aside from this interesting result, the remaining three factors have very predictable influences on the mass transfer to reaction rate resistance ratio as illustrated in Figure 16.

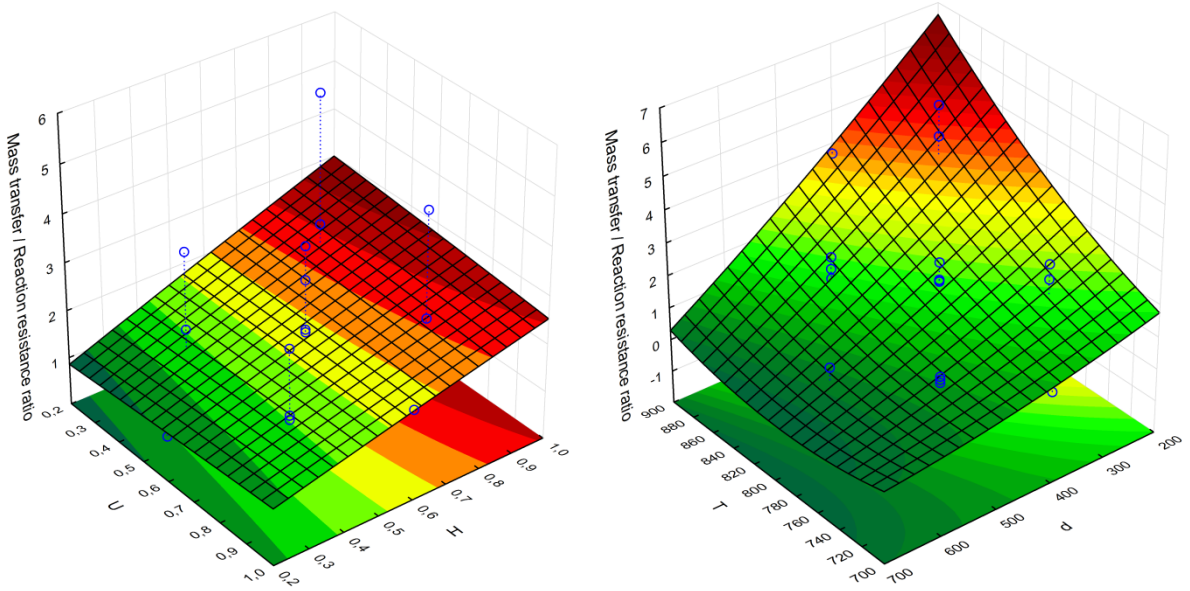

Figure 16: Response of the ratio of mass transfer to reaction rate resistance to changes in the four factors under consideration.

Figure 16 indicates that increases in the static bed height increase the mass transfer resistance as a result of the increased bubble growth associated with taller beds. An increase in reaction temperature is shown to cause a sharp increase in the ratio of mass transfer to reaction rate resistance due to the exponential reduction in reaction rate resistance with increases in temperature.

Of particular interest, however, is the linear reduction in mass transfer resistance with an increase in particle size. Table 6 indicates that this effect is larger even than that of the temperature and Figure 16 shows that a factor three increase in the particle size can cause a factor five reduction in mass transfer resistance at high temperatures. This highly significant effect could be of great industrial interest.

Of course, this effect will only be attractive for porous particles such as those investigated in this study where the reaction takes place on grains throughout the particle instead of on the surface of the particle itself, implying negligible mass transfer resistance inside the particle and making reaction rate resistance independent of particle size. Many particles exhibit this kind of behavior (e.g. [19, 20]) and this assumption can remain valid up to particle sizes of 1 mm or more [21].

It can therefore be very interesting to further investigate how this effect can be best exploited to ensure minimal mass transfer resistance in dense fluidized bed reactors. Proper utilization of this factor could be an important consideration in reactor optimization studies.

7 Conclusions

CFD simulations of a bubbling fluidized bed reactor were carried out on a 2D planar and 3D cylindrical geometry using the classical two fluid model approach closed by the kinetic theory of granular flows.

Both sets of simulations were completed over a wide parameter space defined by four independent variables: fluidization velocity, bed mass, reactor temperature and particle size.

Simulations showed that the 2D approximation greatly over-predicted reactor performance despite being qualitatively representative. The amount of difference between the 2D and 3D simulations also varied substantially with changes in all four independent variables investigated.

Two primary 2D errors were identified: incorrect predictions of the gas residence time by misrepresentations of the bed expansion and incorrect predictions of the mass transfer by misrepresentations of bubble formation and especially the splash zone at the top of the bed. 2D simulations also predicted a significantly stronger recirculatory flow pattern than 3D simulations, but the influence of this discrepancy on reactor performance could not be directly quantified.

The bed expansion was increasingly misrepresented by the 2D simulation as the degree of core-annular flow structure was increased. This phenomenon occurred because the accumulation of solids near the walls can be accommodated within a shorter bed height in a 3D cylindrical geometry than in a 2D planar geometry. The degree of core-annular flow, and thereby the bed expansion over-prediction by the 2D model, increased with increases in fluidization velocity and decreases in particle size. Differences in the bed expansion ratio influenced the gas residence time and therefore also the reactor performance.

The mass transfer error was even more influential than the residence time error though. At low flowrates, the small bubbles forming near the distributor could not be resolved in 2D, leading to significant over-predictions of the gas-solid contact and therefore also the reactor performance. In addition, the splash region at the top of the bed was found to result in much greater conversion in 2D since the missing degree of freedom prevented the gas from exiting cleanly out the top of the bed.

Mass transfer predictions were affirmed as the most important factor to be captured by simulations and were analysed further. It was shown that the use of larger particle sizes could be a very promising way to improve reactor performance when porous particles with negligible internal mass transfer resistance are used. For example, an increase in particle size from 200 to 600 microns caused a five times reduction in the mass transfer resistance.

In closing, it is highly recommended that 2D simulations only be employed for model testing and rapid prototyping of new concepts. 3D simulations were found to be mandatory for any application where acceptable quantitative predictions are required.

8 Acknowledgement

The authors would like to acknowledge the financial support from the Research Council of Norway. The authors are also grateful for the use of the supercomputing facilities at the Norwegian University of Science and Technology for running the large number of expensive 3D simulations required by this study.

9 References

[1] Cloete S, Amini S, Johansen ST. On the effect of cluster resolution in riser flows on momentum and reaction kinetic interaction. Powder Technology. 2011;210(1):6-17.

[2] Igci Y, Andrews AT, Sundaresan S, Pannala S, O'Brien T. Filtered two-fluid models for fluidized gas-particle suspensions. AIChE Journal. 2008;54(6):1431-48.
[3] Cloete S, Amini S, Johansen ST. A fine resolution parametric study on the numerical simulation of gas-solid flows in a periodic riser section. Powder Technology. 2011;205(1-3):103-11.
[4] Syamlal M, Rogers W, O'Brien TJ. MFIX Documentation: Volume 1, Theory Guide. Springfield: National Technical Information Service 1993.
[5] Lun CKK, Savage SB, Jeffrey DJ, Chepurniy N. Kinetic Theories for Granular Flow: Inelastic Particles in Couette Flow and Slightly Inelastic Particles in a General Flow Field. Journal of Fluid Mechanics. 1984;140:223-56.
[6] Gidaspow D, Bezburuah R, Ding J. Hydrodynamics of Circulating Fluidized Beds, Kinetic Theory Approach. *7th Engineering Foundation Conference on Fluidization* 1992:75-82.
[7] Van Wachem BGM, Schouten JC, Van den Bleek CM, Krishna R, Sinclair JL. Comparative analysis of CFD models of dense gas-solid systems. AIChE Journal. 2001;47(5):1035-51.
[8] Schaeffer DG. Instability in the Evolution Equations Describing Incompressible Granular Flow. Journal of Differential Equations. 1987;66:19-50.
[9] Ogawa SU, A.; Oshima, N. On the Equation of Fully Fluidized Granular Materials. Journal of Applied Mathematics and Physics. 1980;31:483.
[10] Levenspiel O. Chemical Reaction Engineering. 3 ed: John Wiley & Sons 1999.
[11] Johnson PC, Jackson R. Frictional-Collisional Contitutive Relations for Granular Materials, with Application to Plane Shearing. Journal of Fluid Mechanics. 1987;176:67-93.
[12] Patankar S. Numerical Heat Transfer and Fluid Flow: Hemisphere Publishing Corporation 1980.
[13] Leonard BP, Mokhtari S. ULTRA-SHARP Nonoscillatory Convection Schemes for High-Speed Steady Multidimensional Flow. NASA TM 1-2568 (ICOMP-90-12); 1990; NASA Lewis Research Center; 1990.
[14] Taghipour F, Ellis N, Wong C. Experimental and computational study of gas-solid fluidized bed hydrodynamics. Chemical Engineering Science. 2005;60(24):6857-67.
[15] Montgomery D. Design and Analysis of Experiments. 5 ed. New York: John Wiley and Sons 2001.
[16] Cloete S, Amini S. Mapping of the Operating Window of a Lab Scale Bubbling Fluidized Bed Reactor by CFD and Designed Experiments. 8th International Conference on CFD in the Oil & Gas, Metallurgical and Process Industries 2011 21-23 June 2011; Trondheim, Norway; 2011.
[17] Cloete S, Johansen ST, Amini S. An assessment of the ability of computational fluid dynamic models to predict reactive gas–solid flows in a fluidized bed. Powder Technology. 2012;215-216(0):15-25.
[18] Pröll T, Kolbitsch P, Bolhàr-Nordenkampf J, Hofbauer H. A novel dual circulating fluidized bed system for chemical looping processes. AIChE Journal. 2009;55(12):3255-66.
[19] Abad A, Adánez J, Cuadrat A, García-Labiano F, Gayán P, de Diego LF. Kinetics of redox reactions of ilmenite for chemical-looping combustion. Chemical Engineering Science. 2011;66(4):689-702.
[20] García-Labiano F, Adánez J, de Diego LF, Gayán P, Abad A. Effect of Pressure on the Behavior of Copper-, Iron-, and Nickel-Based Oxygen Carriers for Chemical-Looping Combustion. Energy & Fuels. 2005;20(1):26-33.
[21] Abad A. Personal communication. 2010.